Competitive adsorption property of multi-metals in static and dynamic process using millet chaff-based biochar

Zehua Ji, Yuansheng Pei*

The Key Laboratory of Water and Sediment Sciences, Ministry of Education, School of Environment, Beijing Normal University, Beijing 100875, China, Tel. +86 18811081174; emails: yspei@bnu.edu.cn (Y. Pei), jizehua2010@163.com (Z. Ji)

ABSTRACT

Waste millet chaff-based biochar (MCB) was tested as an alternative adsorbent for the removal of Pb(II), Zn(II) and Cd(II) from the multicomponent (unitary, binary and ternary) systems in static and dynamic conditions. In static adsorption study (batch experiment), the adsorption process of three cations followed the Langmuir and Dubinin–Radushkevich models, and the theoretical maximum adsorption capacity (q_m) of MCB for different heavy metals followed the order of Pb(II) (0.5097 mmol g^{-1}) > Zn(II) (0.2466 mmol g^{-1}) > Cd(II) (0.1948 mmol g^{-1}). In binary and ternary systems, Pb(II), Zn(II) and Cd(II) showed more significant inhibition effect on the co-existence ions' adsorption in higher initial concentration, and the competitive effect of Pb(II) was the strongest. In dynamic adsorption study (fixed-bed experiment), the dynamic adsorption capacity (q_d) of MCB for three cations followed the order of Pb(II) (0.4526 mmol g^{-1}) > Zn(II) (0.2369 mmol g^{-1}) > Cd(II) (0.2024 mmol g^{-1}), and the parameters of dynamic systems were also significantly influenced by the cations. Based on the results of model calculation, the Thomas model can be used to describe the dynamic adsorption process of Pb(II) in multicomponent systems and Zn(II) (or Cd(II)) in unitary systems.

Keywords: Waste millet chaff biochar; Heavy metals; Competitive adsorption; Fixed bed; Thomas model

1. Introduction

Among various water treatment technologies, adsorption has been widely regarded as a simple, flexible and highly efficient method to remove heavy metal from industrial effluents and natural wastewater [1,2]. Up to date, biochar have been extensively researched as an efficient and cost-effective adsorbent for the adsorption treatment of pollutants [3]. The application of forestry and agricultural residues as row materials of biochar both solves the treatment problem of the waste solid and provides a large number of reliable sources for adsorbent. Thus, as a promising method for treating wastewater containing heavy metals, the waste-based biochar has been widely accepted and researched in recent years [4–7].

At the current stage, the most of researches on adsorption of metal ions by biochar are focused on discontinuous batch experiments under the mono metal system, and there were a few studies on the competitive adsorption of multi-metals in dynamic process [8]. In the static adsorption, the adsorbent reacts with the constant liquid, which can be used to test the adsorption performance of adsorbent, but cannot be directly applied in practical treatment process. The dynamic adsorption occurs in the system with dynamic flow, the continuous contaminated flow passes through the reactor (e.g., fixed bed, fluid bed) and the contamination is dynamically adsorbed by the adsorbent. The fixed-bed reactor is a commonly used dynamic adsorption technology for the continuous flow with pollutants in the practical treatment process [9]. For better design and control of fixed-bed system in water treatment, it is necessary to focus on the different pollutant and system parameters in reactor. Furthermore, both in practical

* Corresponding author.

wastewaters and natural streams, the presence of only one ion is a rare situation and the treatment process is always in the continuous condition. So the interfacial adsorption behavior in complex and dynamic condition can directly influence the fate and treatment efficiency of heavy metal. And in multiple ions system, the adsorption mechanisms are complex and significantly influenced by the coexisting ions [10,11]. Based on these characteristics, the research about the multiple ions solutions system is contribute to ascertain adsorption behaviors in practical situation and the interaction mechanism of cations.

Millet is an important crop in Asia and Africa, and nearly 30 million tons of millet is produced annually. Millet chaff is a by-product in millet processing, which is one of few researched biomass resource, and its subsequent utilization has great potential in heavy metal adsorption [8,12]. Our pre-experiment result [12] and the present study demonstrated that carbonization process can significantly improve the adsorption capacity of millet chaff for Pb^{2+} (0.5097 mmol g^{-1} rather than 0.0574 mmol g^{-1}), the millet chaff biochar presents a better adsorption property. Before proceeding to practical application, it is necessary to elucidate the adsorption behaviors of heavy metals in both static and dynamic systems.

In order to elucidate the adsorption behaviors of heavy metals in static system (batch experiment) and dynamic system (fixed-bed reactor), the effect of multi-components, ionic strength and static/dynamic systems on the adsorption of Pb(II), Zn(II) and Cd(II) was investigated in this study. Furthermore, adsorption models (e.g., Langmuir, Freundlich, Temkin, Dubinin–Radushkevich and Thomas model) were used in different adsorption conditions to further analyze the adsorption mechanisms in complex system.

2. Materials and methods

2.1. Millet chaff pyrolysis for biochar production

The waste millet chaff (MC) was collected from a local agricultural field in Gongyi city, Henan province, China, and used to produce biochar. A muffle furnace was used to convert the sample into biochar under a limited oxygen condition. Millet chaff biochar (MCB) was produced at 400°C for 4.0 h in airtight crucible. The MCB produced in this work was crushed and sieved to <0.38 mm.

2.2. Static regime adsorption experiment

All chemical reagents used in this study [$Pb(NO_3)_2$, $Zn(NO_3)_2 \cdot 6H_2O$, $Cd(NO_3)_2$] were of analytical grade reagents and supplied by Xi Long chemical Co. Ltd., (Guangdong, China). All solutions were prepared with ultra pure water. The static regime adsorption experiment of Pb(II), Zn(II) and Cd(II) ions was studied by the batch method under the same conditions as below. Unitary adsorption of Pb(II), Zn(II) and Cd(II) ions was obtained by weighing 0.1 g of MCB for each test in glass Erlenmeyer flasks, and then, 50 mL of solutions containing specific concentrations (0.50, 0.75, 1.00, 1.25 and 1.50 mmol L^{-1}) of the metal ions were added to the flask. The pH of the solutions were adjusted to pH 5.5 using 0.1 M HNO_3 or 0.1 M NaOH solutions. The Erlenmeyer flasks were then incubated on a rotary shaker (THZ–C, Huamei biochemical instrument, China) for 24 h (time setting based on the result

of pre-experiment) at 28°C. After that, suspensions were filtered through a filter paper of 0.45 μm. Ultimately, Pb(II), Zn(II) and Cd(II) ions concentration in the aqueous phase was measured by atomic absorption spectrometry (AAS3500, Thermo Electron Corporation, USA).

Binary and ternary adsorption experiment was conducted with different multi-metal solutions ((1) Pb–Zn; (2) Pb–Cd; (3) Zn–Cd and (4) Pb–Zn–Cd) with varying initial concentrations (0.50, 0.75, 1.00, 1.25 and 1.50 mmol L^{-1}). The pH, adsorption time, adsorbent dosage, temperature and rotary speed were the same as unitary metal adsorption experiment.

In batch experiment, the equilibrium adsorption capacity (q_e, mmol g^{-1}) was calculated by the Eq. (1):

$$q_e = \left(C_0 - C_e \right) \times \frac{V}{m} \tag{1}$$

where V is the volume of the solutions (L), m is the weight of the MCB (g), C_0 is the initial concentration of heavy metal ion and C_e is the equilibrium concentration of heavy metal ion. In order to ensure the accuracy and reliability of the data in this study, experiments we carried out in triplicate and mean values of the triplicate were used for analysis.

2.3. Dynamic adsorption experiment

The dynamic unitary adsorption experiments were carried out in fixed-bed (internal diameter = 10 mm and length = 250 mm) with 1,250 mg MCB, and glass wool was supported in the column (10 mm) to ensure good liquid distribution. The solutions containing specific concentration (1.00 mmol L^{-1}) of the metals (only Pb(II) or Zn(II) or Cd(II)) were pumped through the column using a peristaltic pump (KCP3-X, Kamoer, Shanghai) with a flow rate of 3.0 mL min^{-1}. The effluent solutions were collected at 10 min intervals and measured by atomic absorption spectrometry. In this research, the breakthrough time (t_b) and exhaustion time (t_e) of fixed-bed adsorption system were defined as effluent concentrations (C_t) equal to 10% C_0 and 95% C_0, respectively.

The fixed-bed binary and ternary adsorption experiment were performed in the same condition with mono-metal experiments. The solutions containing specific concentration (1.00 mmol L^{-1}) of the four combinations of Pb(II), Zn(II) and Cd(II) (namely, (1) Pb–Zn; (2) Pb–Cd; (3) Zn–Cd and (4) Pb–Zn–Cd) were pumped through the column, and the effluents were also collected and analyzed. All experiments were performed in triplicate.

2.4. Adsorption isotherm models

In order to compare the adsorption behaviors of different ions, the maximum adsorption capacity was predicted and mechanisms of adsorption were determined, the experimental data were described by Langmuir, Freundlich, Temkin and Dubinin–Radushkevich (D-R) isotherm models, according to Eqs. (2)–(5), respectively.

$$\frac{C_e}{q_e} = \frac{1}{q_m} K_L + \frac{C_e}{q_m} \tag{2}$$

$$\ln q_e = \ln K_F + \frac{1}{n}\ln C_e \tag{3}$$

$$q_e = A + B\ln C_e, \quad A = \frac{\left[RT\ln K_{Te}\right]}{b}, \quad B = \frac{RT}{b} \tag{4}$$

$$\ln q_e = \ln q_m - \beta\varepsilon^2, \quad \varepsilon = RT\ln\left(1 + \frac{1}{C_e}\right) \tag{5}$$

where C_e is the equilibrium concentration of heavy metal ions in solutions (mmol L^{-1}), q_m is the theoretical maximum adsorption capacity (mmol g^{-1}), R is the thermodynamic equilibrium constant ($R = 8.314$ J mol^{-1} K^{-1}), T is the absolute temperature (K), K_L, K_F, K_{Te}, n, b and β are the constants of different models.

2.5. Calculation of fixed-bed parameters

In fixed-bed experiment, the total mass of metal adsorbed by fixed bed (M_{ad}, mmol), the dynamic adsorption capacity (q_d, mmol L^{-1}), the height of mass transfer zone (H), the total mass of metal through fixed bed (M_{total}, mmol) [13], the total metal removal rate (R, %) and the total solution volume (TV, mL) were defined in Eqs. (6)–(11), respectively.

$$M_{ad} = \frac{Q}{1,000}\int_0^{t_e}\left(C_0 - C_t\right)dt \tag{6}$$

$$q_d = \frac{M_{ad}}{m} \tag{7}$$

$$H = \frac{C_0 \times Q\left(t_e - t_b\right)}{\left(1,000\rho \times q_d \times A\right)} \tag{8}$$

$$M_{total} = \frac{C_0 \times Q \times t_{total}}{1,000} \tag{9}$$

$$R = \frac{M_{ad}}{M_{total}} \tag{10}$$

$$TV = t_e \times Q \tag{11}$$

where Q is the velocity of liquid (mL min^{-1}), C_0 and C_t are the heavy metal ions' concentration (mg L^{-1}) in aqueous solutions of inlet and outlet, respectively, m is the weight of the MCB in fixed bed (g), t_b and t_e are the time (min) of breakthrough point and exhaustion point, respectively, ρ is the packed density (g cm^{-3}) of MCB, A is the cross-sectional area of fixed bed (cm^2).

The Thomas model was used for the analysis of breakthrough curves' characteristics and the linear form of model was given by Eq. (12):

$$\frac{C_t}{C_0} = \frac{1}{\left[1 + \exp\left(K_{th}q_{md} \times m / Q - K_{th}C_0 \times t\right)\right]} \tag{12}$$

where K_{th} is the Thomas model rate constant (10^{-3}L min^{-1} mmol^{-1}), q_{md} is the theoretical maximum dynamic adsorption capacity (mmol g^{-1}).

2.6. Characterization of MC and MCB

In order to confirm the change of MC and MCB through the carbonization process, the morphologies of the MC and MCB were analyzed via scanning electron microscopy (SEM) and Fourier transform infrared spectroscopy (FTIR). The surface morphologies of two materials were obtained by SEM (Quanta450, FEI, USA) at room temperature. And the FTIR spectra were obtained using IRAffinity-1 (Shimadzu, Japan) and the spectra were recorded in 400–4,000 cm^{-1} range. The specific surface area and pore size distribution of material and biochar were measured by the Brunauer–Emmett–Teller (BET) analysis. The point of zero charge (pH$_{pzc}$) of raw material and biochar was obtained by measuring the equilibrium pH of suspension and plotting the mass titration curve. The cation exchange capacity (CEC) was measured by sodium saturation method. The binding energy of C 1s and O 1s of the MC and MCB was characterized by X-ray photoelectron spectroscopy (XPS, Shimadzu, Japan), and the crystalline phase of the sample was conducted by X-ray diffraction (XRD, PANalytical, Holland).

3. Results and discussion

3.1. Characterizations analysis

In order to describe the property changes of raw materials and biochar, they were characterized using different characterization methods. As shown in Table 1, compared with MC, BET surface area, pore volume and CEC of MCB are all significantly enhanced by carbonization. These changes of parameters mean that the adsorbents with better adsorption properties [6]. SEM analysis of the MC and MCB was performed to determine the different surface characteristics under carbonization process. The MC has a relatively smooth surface, non-porous and columnar structure (Fig. 1a), and the MCB has a rough multilayer surface morphology and considerable numbers of cavities and pores (Fig. 1b). Fig. 1 demonstrated that carbonization process dramatically change the surface characteristics of millet chaff, this result can be attributed to the loss of volatile substances in carbonization process [14,15]. Hassan et al. [10] and Fan et al. [16] have reported that the surface characteristics of different biomass materials can be significantly changed by carbonization, which is consistent with the results of this study.

The FTIR results of MC and MCB are shown in Fig. 2. The FTIR broad absorption band around 3,400 cm^{-1} was

Table 1
Physicochemical characteristics of MC and MCB

Materials	MC	MCB
BET surface area (m^2 g^{-1})	10.540	47.213
Pore volume (cm^3 g^{-1})	0.013	0.027
Micropore area (m^2 g^{-1})	7.240	37.820
Mesopore area (m^2 g^{-1})	2.721	9.189
Total pore volume (cm^3 g^{-1})	0.010	0.018
Pore diameter (nm)	5.232	2.279
pH$_{pzc}$	6.56	8.08
CEC (cmol kg^{-1})	5.66	9.11
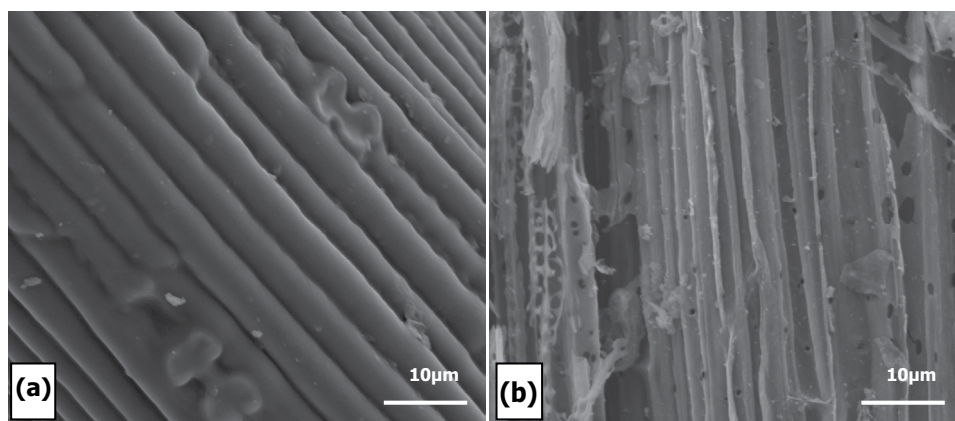
Fig. 1. SEM pictures of (a) millet chaff – MC and (b) MC based-biochar – MCB.
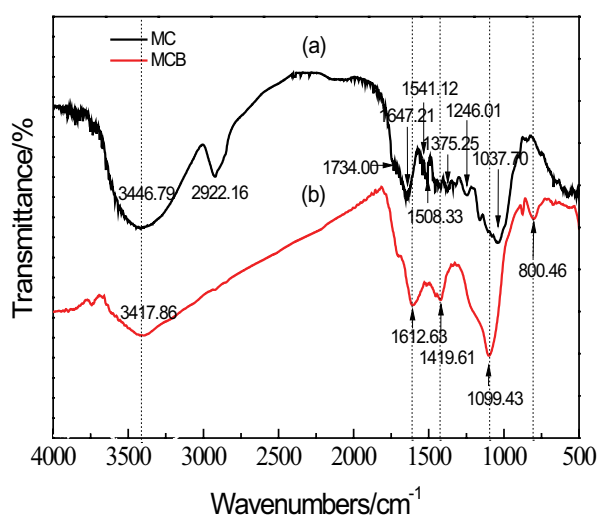
Fig. 2. FTIR pictures of millet chaff and biochar (curve a. millet chaff, curve b. millet chaff biochar).

assigned to stretching vibration of O–H and N–H functional groups, the band around 2,922 cm^{-1} could be assigned to the C–H asymmetrical stretch vibration bond in CH and CH$_2$, the relatively sharp band around 1,647 cm^{-1} could be attributed to stretching vibration of aromatic rings [17]. Other bands observed at 1,541; 1,419 and 1,037 cm^{-1} may correspond to bending vibrations of N–H, bending vibrations of O–H and stretching vibration of C–O, respectively [18,19]. The absorption bands location and categories were changed after carbonization, and formed a new band at 800 cm^{-1}, which could be assigned to the characteristic band of the heterocyclics (e.g., azine, furan) [20]. The crystalline phase information of raw material and biochar was identified by XRD measurement. As shown in Fig. 3a, the raw material and biochar showed typical amorphous spectra [6], and the peaks for MCB at 28° and 40° indicated that the presence of sylvite (KCl, PDF# 41-1476) [21]. XPS was used to provide the elemental composition of C and O. Deconvolution of the C 1s spectrum before and after the carbonization were presented in Fig. 3c (MC) and Fig. 3d (MCB), respectively. Compared with the MC, more peaks of C 1s (C=O and O–C=O) were showed in the spectrum of MCB, indicating that more functional groups

were generated in the carbonization process [22], and this result is consistent with the result of FTIR.

3.2. Adsorption in unitary system

The effect of initial concentration (C_0) on adsorption capacity in unitary system is shown in Fig. 4. As presented in the figure, the adsorption capacities at equilibrium (q_e) for different ions were increased with increasing C_0, and the value of q_e reached a plateau when C_0 was above 1.0 mmol L^{-1}. This change with C_0 was due to higher initial concentration that provides stronger driving force for ion to overcome mass transfer resistances between the aqueous and solid phases [17,23]. It is clear that the adsorption capacity of MCB for different ions followed the order: Pb(II) > Zn(II) > Cd(II), and this adsorption affinity for Pb(II) is significantly higher than those of Zn(II) and Cd(II). Similar order has been published by many researches [4,14,24,25], which implied that Pb(II) could bind with more varieties of adsorption sites [26].

The Langmuir, Freundlich, Temkin and D-R models were used to describe the data of experiment. All parameters and regression coefficients R^2 were calculated and summarized in Table 2. Among all these models, Langmuir model best fitted the experimental data with a correlation coefficient value ($R^2 = 0.9987 - 0.9998$) close to 1, suggesting that the adsorption processes of heavy metals on the MCB are mainly controlled by single molecular adsorption [27,28]. The values of q_m of Pb(II), Zn(II) and Cd(II) are 0.51, 0.25 and 0.19 mmol g^{-1}, respectively. The R^2 ($0.9439 - 0.9968$) of D-R model indicated that this model also can be used to describe the adsorption processes. Generally, the D-R model was based on Polanyi adsorption theory, which implied that the volume filling theory of micropores is the main mechanism of adsorption [29]. As shown in Fig. 1b, the surface of MCB is full of cavities and pores, which provided opportunities for the volume filling. Based on fitting results and SEM picture, we can conclude that the volume filling effect plays a vital role in adsorption process on the MCB. The Freundlich model was used to describe the adsorption of a reversible heterogeneous surface and not restricted to monolayer adsorption [30]. And the Temkin model explicitly takes into account the adsorbent–adsorbate interactions, and assumed that the heat of adsorption of all molecules decrease linearly with coverage [31]. In this study, the R^2 values of Freundlich and Temkin model are
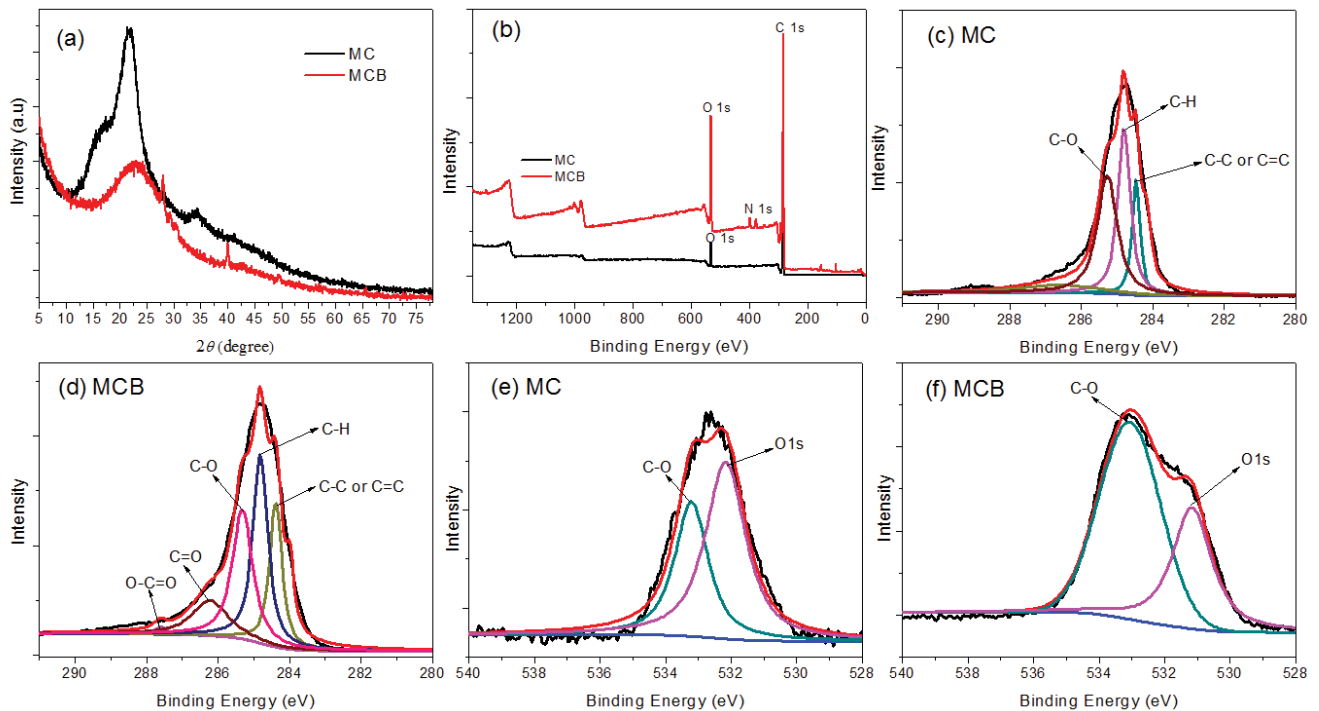
Fig. 3. X-ray diffraction pattern (a) and XPS spectrum of MC and MCB, (b) wide spectrum, (c) C1s of MC, (d) C1s of MCB, (e) O1s of MC, and (f) O1s of MCB.
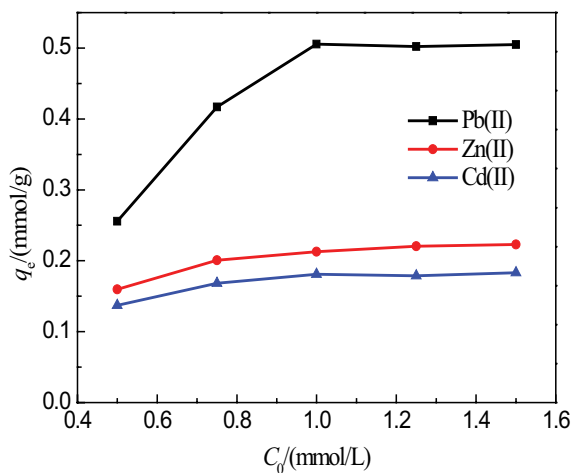
Fig. 4. Effect of initial concentration on adsorption capacities of different heavy metal ions.

lower than that of Langmuir and D-R model. Consequently, Langmuir and D-R model are more suitable to describe the Pb(II), Zn(II) and Cd(II) adsorption processes on MCB.

Many published researches by Du et al. [32], Fan et al. [33], and Park et al. [34] have reported the competitive adsorption effect on various adsorbents. Regardless of the different materials, the adsorption capacity for Pb(II) in their studies was always better than Zn(II), Cd(II) and Cu(II). It can be concluded that the reason for this affinity is not due to the difference of adsorbent, but on the formation of cations in aqueous solution. Generally, the main pattern of metallic cation exists in aqueous solutions is hydrated cation

($Cd(H_2O)_6^{2+}$, $Pb(H_2O)_6^{2+}$, and $Zn(H_2O)_6^{2+}$) [35]. The water molecules in metallic hydrated cation can be replaced by OH$^-$ in different pH and generate various hydrated speciation ($Cd(OH)_2$, $Cd(OH)_3^-$, $PbOH^+$, $Pb_2(OH)_3^+$, $Pb_4(OH)_4^{4+}$, $ZnOH^+$, $Zn_2(OH)_3^+$, etc.) [36]. Once metal dissolves into the aqueous solution, metallic cation forms hydrated ion with molecule of water, and the hydrated ionic radius of Pb(II), Zn(II) and Cd(II) are 0.401, 0.430 and 0.426 Å, respectively [37]. It can be deduced that the main adsorption forms of metal ions are hydrated cation, and q_m for different ions are directly affected by hydrated ionic radius. The hydrated ionic radius of Zn(II) and Cd(II) is very close to the other one, and that of Pb(II) is obviously lower than the former two. Consequently, the preferential adsorption of Pb(II) may be based on its smaller hydrated ionic radius. From the above research results, the three possible mechanisms for the adsorption capacity difference of different ions are: (i) the hydrated ion quantity of different cations is different with same initial concentration, (ii) the different hydrated ion occupied different adsorption sites, the smaller the ionic radius, the more the number of hydrated ions that will occupy the given site, and (iii) the existence of non-specific sites and specific sites, the latter only adsorb the specific ion.

3.3. Competitive adsorption behavior in binary and ternary metal system

Fig. 5 shows the values of q_e of Pb(II), Zn(II) and Cd(II) in different mixture components. Interaction effect between Pb(II) and Zn(II) is given in Fig. 5a. The experimental data indicates that the values of q_e of Pb(II) and Zn(II) at binary systems are significantly lower than those in single-solute systems. The adsorption inhibition effect of Pb(II) on Zn(II) was

Table 2
Parameters of different isotherms for the adsorption of Pb(II), Zn(II) and Cd(II)

Ions	Langmuir			Freundlich			Temkin			D-R		
	q_m	K_L	R^2	n	K_F	R^2	A	B	R^2	q_m	β	R^2
Pb(II)	0.5097	0.0067	0.9998	5.8207	0.5826	0.8028	0.5570	0.0628	0.8018	0.5490	7.00E-09	0.9439
Zn(II)	0.2466	0.1128	0.9995	4.8008	0.2252	0.9585	0.2240	0.0395	0.9699	0.2357	2.00E-08	0.9968
Cd(II)	0.1948	0.0883	0.9987	6.2344	0.1785	0.8702	0.1787	0.0256	0.8831	0.1916	2.00E-08	0.9778
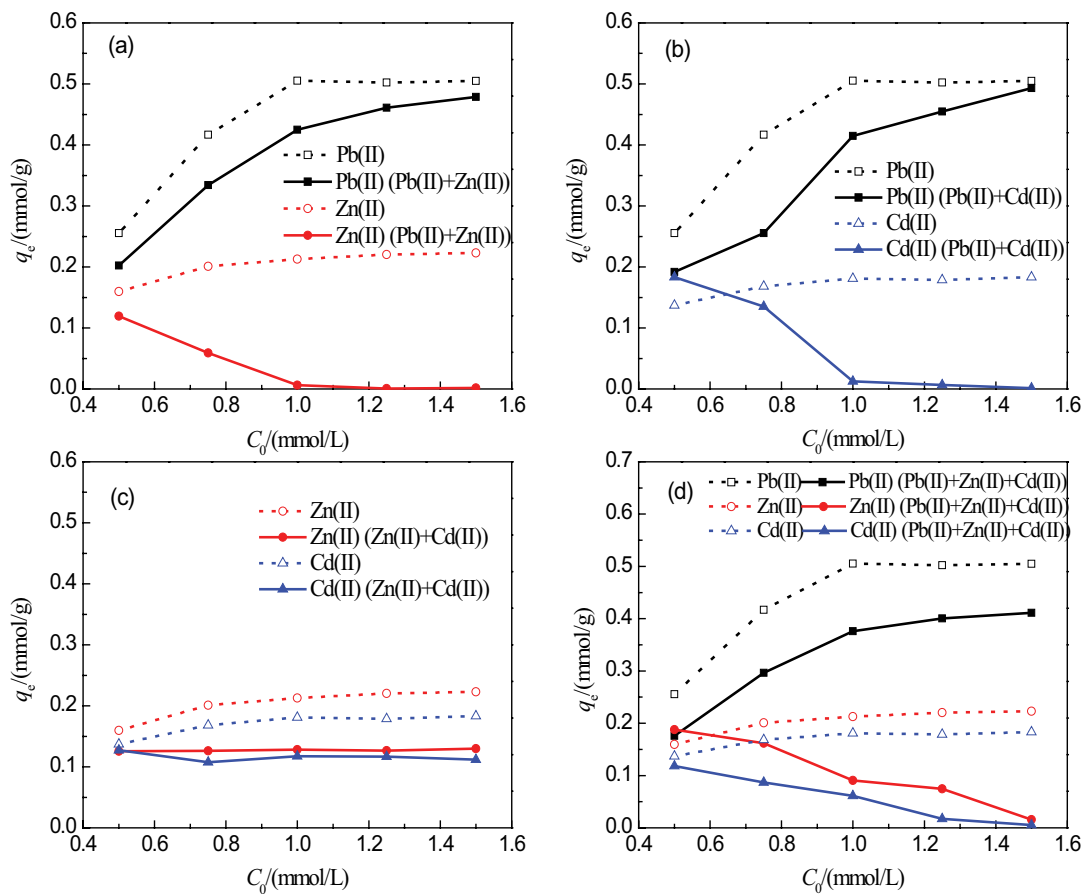
Fig. 5. Static adsorption capacities of heavy metal ions in different mixture components (Dotted line: q_e of heavy metal in unitary system; Real line: q_e of heavy metal in multi-compound system). (a) Pb-Zn binary system, (b) Pb-Cd binary system, (c) Zn-Cd binary system, and (d) Pb-Zn-Cd ternary system.

increased with increasing initial concentration. Subsequently, at the C_0 exceeded 1.0 mmol L^{-1}, the value of q_e of Zn(II) was reduced to nearly zero. Furthermore, as the C_0 increased, the inhibition effect of Zn(II) on Pb(II) was attenuated, and the value of q_e of Pb(II) at binary-solute was gradually close to that of single-solute system.

Fig. 5b depicts the values of q_e for Pb(II) and Cd(II) in the presence of the other one. Compared with the Fig. 5a, the adsorption inhibition effect variation tendency of Pb–Cd binary system was similar to that of Pb–Zn system. This result implies that Pb^{2+} ion has a stronger adsorption inhibition effect on Zn(II) and Cd(II) at the same concentration. As shown in Fig. 5b, the change of q_e in Pb–Cd system was

slightly bigger than in Pb–Zn system, which indicates that the interaction effect of Pb(II) between Cd(II) was weaker than Pb(II) between Zn(II).

The interaction of Zn(II) and Cd(II) is shown in Fig. 5c. The values of q_e of Zn(II) and Cd(II) at binary were all lower than the unitary system. In comparison with the single-solute system, the values of q_e of Zn(II) and Cd(II) were declined about 50% and 40%, respectively. Unlike the inhibition effect of Pb(II) on Zn(II) and Cd(II), the presence of Zn(II) or Cd(II) does not strongly inhibit the other ions adsorption. The values of q_e of Zn(II) and Cd(II) are approximately constant in Fig. 5c, which can be ascribed to the finite amount of specific sites and similar ionic radius of the two ions. Under

the joint action of Zn(II) and Cd(II), the specific adsorption sites reached saturation quickly, hence, the value of q_e was no further varying with increasing C_0.

Fig. 5d shows the values of q_e of Pb(II), Zn(II) and Cd(II) in ternary system. The adsorption inhibition effect on Pb^{2+} can be compared with Figs. 5a–c. The q_e decrease of Pb(II) in ternary system was more significant than binary systems, which may be due to the joint inhibition effect of Zn(II) and Cd(II) on Pb(II). Furthermore, as shown in Figs. 5b and d, the values of q_{Cd} and q_{Zn} were promoted at low concentration (0.5 mmol L^{-1}), which may be due to some adsorption sites can be activated by Pb(II), and then those sites are available for the adsorption of Zn(II) and Cd(II).

Above research results reveals that the adsorption affinity of MCB for Pb(II) ion is far higher than Zn(II) and Cd(II), and the inhibition effect of Pb(II) is stronger than other metals. The study of Ding et al. [38] suggested that the metal with a higher adsorption capacity in single metal system exhibit a stronger inhibitory effect on the adsorption of other ions in the multi-metal system. Similarly, Mahamadi and Nharingo [39] studied the competitive adsorption of Pb(II), Cd(II) and Zn(II) ions onto *Eichhornia crassipes* in multi-metal systems. They found that the combined action of the metals was antagonistic, and the metal sorption followed the order of Pb(II) > Cd(II) > Zn(II) in single system, and the biosorption affinity followed the order of Pb(II) >> Zn(II) > Cd(II) in ternary system. These study results are in agreement with our research.

In order to further analyse the quantitative relationship between adsorption capacity in mono- and multi-ions systems, the values of q_e of Pb(II), Zn(II) and Cd(II) (q_{Pb}, q_{Zn}, q_{Cd}) and the total adsorption capacity of adsorbent in batch experiment (q_{st}, $q_{st} = q_{Pb} + q_{Zn} + q_{Cd}$) under different initial concentration and systems are summarized in Table 3. The value of q_m (mmol g^{-1}, calculated by Langmuir model) can be applied to calculation of entire adsorption capacity. Ideally, this parameter is based on the material feature and it is stable when adsorbate has non-interaction with the other factors. However, there is a visible discrepancy between q_m and actual adsorption capacity in multi-components solutions (Fig. 5; Table 1).

As shown in Table 1, the values of q_{Pb} of Pb–Zn and Pb–Cd systems are 0.48 and 0.49 mmol g^{-1}, respectively, which is close to the q_{m-Pb} (0.51 mmol g^{-1}). According to the Table 3, the data indicate that the specific adsorption sites for Zn(II) and Cd(II) not worked under the inhibition effect of Pb(II), which caused the no-growth of total adsorption site in multi-metals system. In Zn–Cd system, the value of q_{st} is
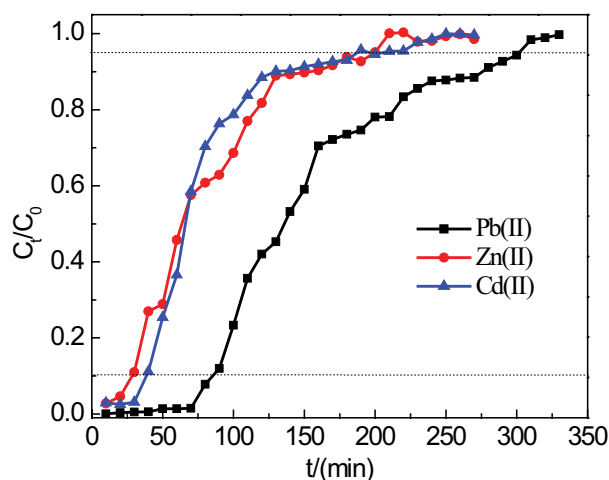
Fig. 6. Breakthrough curves of Pb(II), Zn(II) and Cd(II) on millet chaff biochar.

around 0.23 – 0.25 mmol g^{-1}, which is close to the value of q_{m-Zn} (0.25 mmol g^{-1}). It can be thought that the specific adsorption sites and mechanism for Zn(II) is similar with Cd(II), and the value of q_{st} is steady under the effect of two ions. Under the Pb–Zn–Cd system, the value of q_{st} increased with increasing initial concentration at lower molar concentration. However, the q_{st} showed contrary tendency at higher molar concentration. This phenomenon could be attributed to the fact that at low concentration, the interactions of different metallic cation were relatively weak. Moreover, the specific adsorption sites for three cations retain partial function, which caused the value of q_{st} to exceed the value of q_{m-Pb}. But under the high concentration, the surface of MCB was covered by positively charged cations. Excessive charge accumulation inhibited the cations' adsorption and declined the value of q_{st}.

3.4. Breakthrough curves in unitary system

To design an actual adsorption system, it is necessary to know the information about dynamic adsorption behaviors of the metal ions in the continuous effluent along the time. Fig. 6 shows the breakthrough profiles of Pb(II), Zn(II) and Cd(II), and the relevant parameters were determined and summarized in Table 4. As shown in Fig. 6, the curves demonstrate the relative concentrations (C_t/C_0) on the *y*-axis vs. time (*t*, min) on the *x*-axis. The breakthrough curves shape and location of Pb(II) is different for that of Zn(II)

Table 3
Static adsorption capacities and total adsorption capacities of heavy metal ions in different compound systems

Ion concentration	Pb(II)–Zn(II)	Pb(II)–Cd(II)	Zn(II)–Cd(II)	Pb(II)–Zn(II)–Cd(II)
	q_{st}	q_{st}	q_{st}	q_{st}
0.50	0.3214	0.3751	0.2529	0.4820
0.75	0.3933	0.3903	0.2338	0.5454
1.00	0.4309	0.4273	0.2458	0.5279
1.25	0.4615	0.4613	0.2432	0.4924
1.50	0.4801	0.4945	0.2418	0.4323

Table 4
Breakthrough curve's parameters of Pb(II), Zn(II) and Cd(II)

Ions	t_b/(min)	t_e/(min)	TV/(mL)	M_{ad}/(mmol)	M_{total}/(mmol)	q_d/(mmol g^{-1})	H/(cm)	R/(%)
Pb(II)	86.14	301.33	903.99	0.5658	1.0938	0.4526	6.90	51.73
Zn(II)	28.61	205.4	616.2	0.2961	0.7592	0.2369	11.03	39.01
Cd(II)	38.87	199.33	597.99	0.2530	0.8491	0.2024	13.51	29.79

and Cd(II), but the curve of Zn(II) is analogous to Cd(II). As shown in Table 4, the breakthrough time (t_b) for Pb(II), Zn(II) and Cd(II) was 86.1, 38.9 and 28.6 min, respectively, and the breakthrough exhaustion time (t_e) for Pb(II), Zn(II) and Cd(II) was 301.3, 205.4 and 199.3 min, respectively. The adsorption capacity in fixed bed (q_d) of three ions follows the order: Pb(II) > Zn(II) > Cd(II), this order is same with static q_m. Compared with batch experiment, the adsorbent in fixed-bed system has shorter contact time with adsorbate, which results in less adsorption. However, the results in this study demonstrated that the adsorption capacity of MCB was not decreased significantly in fixed-bed system, indicating that MCB is a suitable material to be used in fixed bed.

In general, height of mass transfer zone (H) is used to reflect the mass transfer resistance of adsorption bed, the shorter H means the weaker mass transfer resistance and the higher utilization rate of bed. Based on Table 3, the value of H of MCB adsorption bed system for Pb(II), Zn(II) and Cd(II) is 6.9, 10.4 and 14.4 cm, respectively. Obtained results showed that the utilization rate of adsorption bed for all three cations follows the order: Pb(II) > Zn(II) > Cd(II).

3.5. Breakthrough curves in different mixture components

Fig. 7 shows the breakthrough profiles of Pb(II), Zn(II) and Cd(II) in different mixture components systems. Interaction effect between Pb(II) and Zn(II) is given in Fig. 7a. In comparison with unitary solution, the breakthrough curves of Pb(II) and Zn(II) in binary system were shifted to left and reached exhaustion point in less time. The curve shape of Pb(II) was hardly changed in binary system, but the curve shape and slope of Zn(II) was obviously changed under the influence of Pb(II). Under the Pb(II)–Cd(II) binary system (Fig. 7b), Cd(II) was also significantly inhibited by the Pb(II) similar to Zn(II). However, unlike Fig. 7b, the curve of Pb(II) showed a slight change in Fig. 7a. This phenomena indicated that the influence of Zn(II) on Pb(II) was more stronger that on Cd(II), which was in agreement with the result of batch experiment. Fig. 7c depicts that the breakthrough curves of Zn(II) and Cd(II) in Zn–Cd system. The breakthrough curves of two cations were apparently left shifted with the shape of curves unchanged. The hydrated ionic radius of Zn(II) and Cd(II) is similar, which make their adsorption, in comparing with the effect of Pb(II), less inhibited by the each other. The competitive adsorption effect in ternary solute system is shown in Fig. 7d. In the presence of all three cations, MCB lost its adsorption effect for Zn(II) and Cd(II) inside in a shorter time. Meanwhile, under the influence of Zn(II) and Cd(II), the breakthrough curve shape of Pb(II) become more flat and trailing. This shape was thought that it was not applicable for fixed-bed adsorption process [40].

Abovementioned results indicated that the Pb(II) has stronger competitive effect than Zn(II) and Cd(II) to the adsorption sites in fixed-bed system, and the competitive effect of Cd(II) is slightly higher than Zn(II). The visible change of Zn(II) and Cd(II) could be mainly attributed to the effect of active adsorption sites was inhibited by Pb(II). Similar findings were also observed by Vinodhini et al. [41] and Sanjoy et al. [42]. Their results proved that multi-metal ions in solutions exerted considerable influence on the adsorption performance of adsorbent, and this influence in batch experiment is consistent with fixed-bed system.

The parameters of breakthrough curve for the different metals are listed in Table 5. Compared with the unitary system, fixed-bed system reached exhaustion point in shorter time at the combined action of all three cations. The data shown in Table 5 revealed that q_d for metal was inhibited by co-existence ion. And the value of H of Zn(II) and Cd(II) was significantly influenced by Pb(II). When Pb(II) existed in solutions, the non-specific sites for three cations were mainly occupied by Pb(II), and the specific sites only interact with Zn(II) or Cd(II). There are a few of specific sites but it possesses special affinity for Zn(II) or Cd(II). This micro-particularity can directly influence the macro-performance of fixed-bed system. Therefore, the existence of specific sites means that the Zn(II) and Cd(II) can be adsorbed more efficiently, which resulted in the decreased of H value in compound system. On the contrary, the H for Pb(II) was increased in multi-metal system. This phenomenon may be due to the obtained parameters of Pb(II), unlike that of Zn(II) or Cd(II), were mainly based on the non-specific sites. When the Zn(II) or Cd(II) existed in solutions, the non-specific sites were occupied. The available fixed-bed utilization rate for Pb(II) was decreased due to the Zn(II) and Cd(II), which led to the increase of H value.

3.6. Thomas model

The results of Thomas model are presented in Fig. 8 and Table 6. As shown in Fig. 8, the fitting curves for Pb(II) adsorption in different systems are analogous. But the fitting curves of breakthrough curves for Zn(II) and Cd(II) produced marked change when Pb(II) existed in system. Through the analysis on Thomas model rate constant (K_{th}) of binary solute system, the K_{th} of Zn(II) and Cd(II) in dynamic adsorption processes were greatly affected by Pb(II), and this numerical change is consistent with the findings of breakthrough curves research [43,44]. Nevertheless, the change of K_{th} in different systems was diverse and irregular. This result was mainly due to the change of breakthrough curve profiles and exhaustion time, which led to the difficulty in applying K_{th} value directly in multi-metals system.
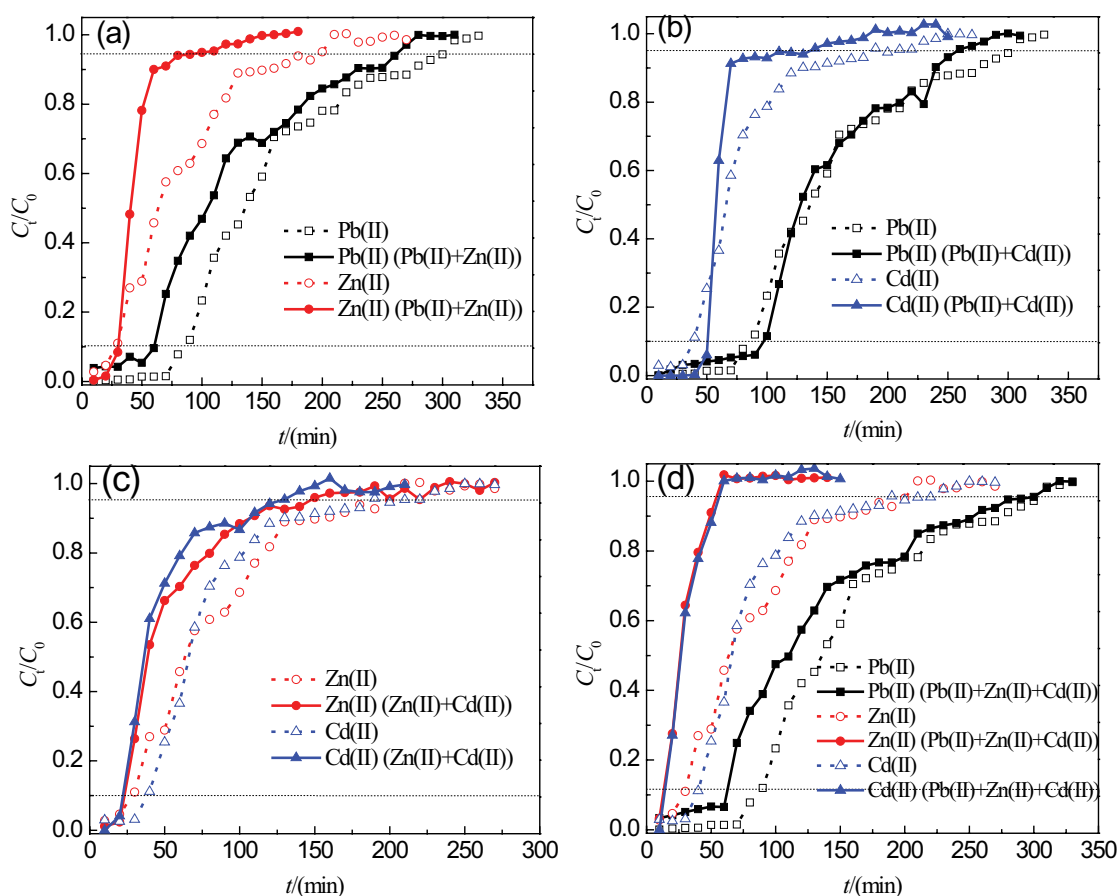
Fig. 7. Breakthrough curves of Pb(II), Zn(II) and Cd(II) in different compound systems (Dotted line: C_t/C_0 of heavy metal in unitary system; Real line: C_t/C_0 of heavy metal in multi-compound system). (a) Pb-Zn binary system, (b) Pb-Cd binary system, (c) Zn-Cd binary system, and (d) Pb-Zn-Cd ternary system.

Table 5
Breakthrough curve's parameters of Pb(II), Zn(II) and Cd(II) in different compound systems

Ions	System	t_b/(min)	t_e/(min)	TV/(mL)	M_{ad}/(mmol)	M_{total}/(mmol)	q_d/(mmol/g)	H/(cm)	R/(%)
Pb(II)	Pb(II)	86.14	301.33	903.99	0.5658	1.0938	0.4526	6.90	48.27
	Pb(II)–Zn(II)	60.31	262.22	786.66	0.3824	0.8732	0.3059	8.79	56.21
	Pb(II)–Cd(II)	96.96	258.55	775.65	0.3823	0.8695	0.3058	7.11	56.03
	Pb(II)–Zn(II)–Cd(II)	61.73	290.6	871.8	0.4114	1.0688	0.3292	10.23	61.50
Zn(II)	Zn(II)	28.61	205.4	616.2	0.2961	0.7592	0.2369	11.03	60.99
	Pb(II)–Zn(II)	30.49	94.62	283.86	0.2275	0.3815	0.1820	5.68	40.37
	Zn(II)–Cd(II)	23.19	147.27	441.81	0.2711	0.5302	0.2169	8.24	48.87
	Pb(II)–Zn(II)–Cd(II)	12.75	53.95	161.85	0.1311	0.2216	0.1049	6.45	40.85
Cd(II)	Cd(II)	38.87	199.33	597.99	0.2530	0.8491	0.2024	13.51	70.21
	Pb(II)–Cd(II)	50.48	135.77	407.31	0.1785	0.6085	0.1428	10.71	70.67
	Zn(II)–Cd(II)	21.99	128.61	385.83	0.1786	0.4973	0.1429	11.54	64.09
	Pb(II)–Zn(II)–Cd(II)	13.84	56.28	168.84	0.1421	0.2487	0.1137	6.60	42.85

Based on the fitting curves in Fig. 8 and the regression coefficients R^2 in Table 6, we can confirmed that the R^2 values (0.9105 – 0.9580) of Pb(II) adsorption process was highest in this study. This result indicated that the axial dispersion effect of Pb(II) ion and its hydrated ion was weaker than those of Zn(II) and Cd(II) [9]. As presented in Figs. 8b and c, the Zn(II) and Cd(II) adsorption were reached saturation in short time in the ternary system, which caused the available points for model fitting to be insufficient. In this case, despite their high R^2 values, these results cannot be used for
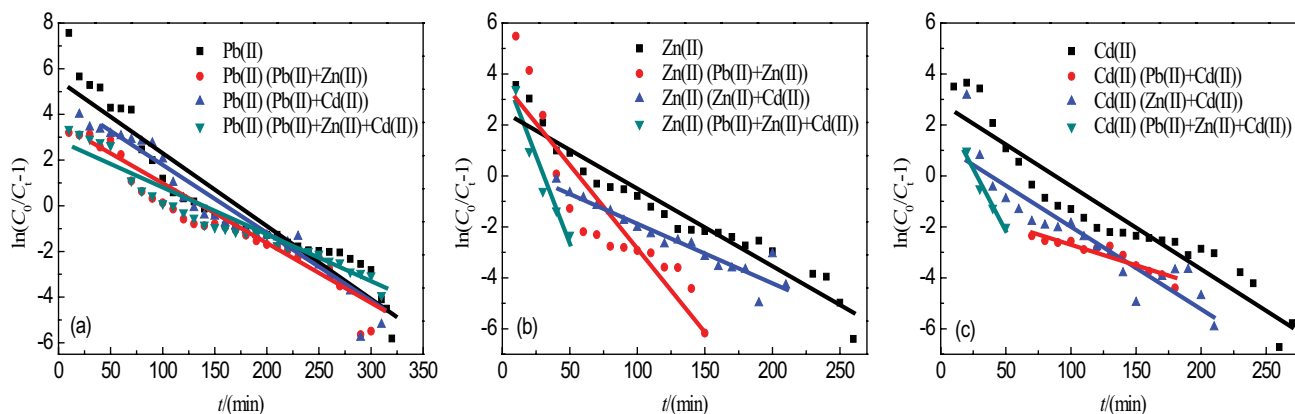
Fig. 8. Linear correlation curves of Thomas model for Pb(II), Zn(II) and Cd(II) in different compound systems.

Table 6
The parameters of Thomas model

Ions	System	$K_{th'}$/(mL min^{-1} mmol^{-1})	q_{md}/(mmol g^{-1})	q_d/(mmol g^{-1})	R^2
Pb(II)	Pb(II)	0.0262	0.5003	0.4526	0.9105
	Pb(II)–Zn(II)	0.0237	0.3379	0.3059	0.9348
	Pb(II)–Cd(II)	0.0275	0.4085	0.3058	0.9580
	Pb(II)–Zn(II)–Cd(II)	0.0175	0.3953	0.3292	0.9401
Zn(II)	Zn(II)	0.0248	0.2485	0.2369	0.9352
	Pb(II)–Zn(II)	0.0491	0.1828	0.1820	0.8341
	Zn(II)–Cd(II)	0.0195	0.0559	0.2169	0.9049
	Pb(II)–Zn(II)–Cd(II)	0.1005	0.0990	0.1049	0.9437
Cd(II)	Cd(II)	0.0231	0.2972	0.2024	0.8998
	Pb(II)–Cd(II)	0.0112	0.2176	0.1428	0.8853
	Zn(II)–Cd(II)	0.0253	0.1211	0.1429	0.8327
	Pb(II)–Zn(II)–Cd(II)	0.0661	0.0986	0.1137	0.9668

direct application. As shown in Table 6, the theoretical maximum dynamic adsorption capacity (q_{md}) was close to q_d when model was used to describe the adsorption process of Pb(II), or the process of Zn(II) and Cd(II) in unitary system. This result implied that the Thomas model can be used to describe the adsorption process of Pb(II) in multi-component system and Zn(II) (or Cd(II)) in unitary systems. However, this model was not applicable to describe the adsorption process of Zn(II)(or Cd(II)) in the multi-component systems.

4. Conclusion

In this study, millet chaff biochar (MCB) was tested as an alternative adsorbent for the removal of Pb(II), Zn(II) and Cd(II) from aqueous solutions. The SEM and FTIR results demonstrated that the surface morphology and functional groups of millet chaff were dramatically changed by carbonization process. In static batch experiment, the q_m of MCB for different heavy metals followed the order of Pb(II) (0.5097 mmol g^{-1}) > Zn(II) (0.2466 mmol g^{-1}) > Cd(II) (0.1948 mmol g^{-1}), it can be deduced that the q_m for different metal ions were directly affected by hydrated ionic radius. The adsorption process of three cations followed the Langmuir

and D-R model. Under the binary and ternary system, Pb(II), Zn(II) and Cd(II) shown inhibition effect on adsorption of co-existence ions, and the competitive effect of Pb(II) was the strongest. In fixed-bed experiment, the q_d for three cations followed the order of Pb(II) (0.4526 mmol g^{-1}) > Zn(II) (0.2369 mmol g^{-1}) > Cd(II) (0.2024 mmol g^{-1}), and the H of Pb(II), Zn(II) and Cd(II) were 6.9, 10.4 and 14.4 cm, respectively. In multi-component systems, the breakthrough curve profiles and parameters were significantly influenced by co-existence cations, and the effects of cation were varied among the different systems. The calculation results implied that the Thomas model can be used to describe the adsorption process of Pb(II) in different systems and Zn(II) (or Cd(II)) in unitary systems. These results indicated that the waste millet chaff-based biochar can be used as an adsorbent for removal of heavy metals in complex aqueous solution.

Symbols

V	–	Volume of the solutions, L
m	–	Weight of the MCB, g
C_0	–	Initial concentration of heavy metal ion, mmol L^{-1}

C_e	–	Equilibrium concentration of heavy metal ion, mmol L^{-1}
q_m	–	Theoretical maximum adsorption capacity, mmol g^{-1}
R	–	Thermodynamic equilibrium constant, $R = 8.314$ J mol^{-1} K^{-1}
T	–	Absolute temperature, K
K_L	–	Constants of Langmuir model
K_F, n	–	Constants of Freundlich model
K_{Te}, b	–	Constants of Temkin model
β	–	Constants of D-R model
M_{ad}	–	Total mass of metal adsorbed by fixed-bed, mmol
q_d	–	Dynamic adsorption capacity, mmol/L
H	–	Height of mass transfer zone, cm
M_{total}	–	Total mass of metal through fixed-bed, mmol
R	–	Removal rate, %
TV	–	Total solution volume, mL
Q	–	Velocity of liquid, mL min^{-1}
C_t	–	Heavy metal ions' concentration in outlet, mmol L^{-1}
t_b	–	Breakthrough point time, min
t_e	–	Exhaustion point time, min
ρ	–	Packed density of MCB, g cm^{-3}
A	–	Cross-sectional area of fixed-bed, cm^2
K_{th}	–	Thomas model rate constant, 10^{-3} L min^{-1} mmol^{-1}
q_{md}	–	Theoretical maximum dynamic adsorption capacity, mmol g^{-1}

Acknowledgments

References

[1] C. Wang, Y. Pei, The removal of hydrogen sulfide in solution by ferric and alum water treatment residuals, Chemosphere, 88 (2012) 1178–1183.

[2] M. Gheju, I. Balcu, G. Mosoarca, Removal of Cr(VI) from aqueous solutions by adsorption on MnO$_2$, J. Hazard. Mater., 310 (2016) 270–277.

[3] Md.A. Islam, M.J. Ahmed, W.A. Khanday, M. Asif, B.H. Hameed, Mesoporous activated coconut shell-derived hydrochar prepared via hydrothermal carbonization-NaOH activation for methylene blue adsorption, J. Environ. Manage., 203 (2017) 237–244.

[4] M. Ahmad, A.U. Rajapaksha, J.E. Lim, M. Zhang, N. Bolan, D. Mohan, M. Vithanage, S.S. Lee, Y.S. Ok, Biochar as a sorbent for contaminant management in soil and water: a review, Chemosphere, 99 (2014) 19–33.

[5] L. Wu, W. Wan, Z. Shang, X. Gao, N. Kobayashi, G. Luo, Z. Li, Surface modification of phosphoric acid activated carbon by using non-thermal plasma for enhancement of Cu(II) adsorption from aqueous solutions, Sep. Purif. Technol., 197 (2018) 156–169.

[6] R.P. Mohubedu, P.N.E. Diagboya, C.Y. Abasi, E.D. Dikio, F. Mtunzi, Magnetic valorization of biomass and biochar of a typical plant nuisance for toxic metals contaminated water treatment, J. Cleaner Prod., 209 (2019) 1016–1024.

[7] B.I. Olu-Owolabi, P.N. Diagboya, E.I. Unuabonah, A.H. Alabi, R.-A. Düring, K.O. Adebowale, Fractal-like concepts for evaluation of toxic metals adsorption efficiency of feldspar-biomass composites, J. Cleaner Prod., 171 (2018) 884–891.

[8] Z. Ji, C. Feng, X. Wu, Y. Li, L. Li, X. Liu, Composite of biomass and lead resistent *Aspergillus oryzae* for highly efficient aqueous phase Pb(II) adsorption, Environ. Prog. Sustainable Energy, 36 (2017) 1658–1666.

[9] A. Abdolali, H.H. Ngo, W. Guo, J.L. Zhou, J. Zhang, S. Liang, S.W. Chang, D.D. Nguyen, Y. Liu, Application of a breakthrough biosorbent for removing heavy metals from synthetic and real wastewaters in a lab-scale continuous fixed-bed column, Bioresour. Technol., 229 (2017) 78–87.

[10] A.F. Hassan, A.M. Abdel-Mohsen, H. Elhadidy, Adsorption of arsenic by activated carbon, calcium alginate and their composite beads, Int. J. Biol. Macromol., 68 (2014) 125–130.

[11] M. Zhu, L. Zhu, J. Wang, T. Yue, R. Li, Z. Li, Adsorption of Cd(II) and Pb(II) by *in situ* oxidized Fe$_3$O$_4$ membrane grafted on 316L porous stainless steel filter tube and its potential application for drinking water treatment, J. Environ. Manage., 196 (2017) 127–136.

[12] Z.H. Ji, C.L. Feng, L. L.G., Adsorption of Pb^{2+} in aqueous solutions by millet chaff: interactive effects between the key factors and mechanism study, Environ. Chem., 36 (2017) 121–132.

[13] S.H. Hasan, D. Ranjan, M. Talat, Agro-industrial waste 'wheat bran' for the biosorptive remediation of selenium through continuous up-flow fixed-bed column, J. Hazard. Mater., 181 (2010) 1134–1142.

[14] J. Wang, C. Chen, Biosorbents for heavy metals removal and their future, Biotechnol. Adv., 27 (2009) 195–226.

[15] L. Lonappan, T. Rouissi, R.K. Das, S.K. Brar, A.A. Ramirez, M. Verma, R.Y. Surampalli, J.R. Valero, Adsorption of methylene blue on biochar microparticles derived from different waste materials, Waste Manage., 49 (2016) 537–544.

[16] S. Fan, J. Tang, Y. Wang, H. Li, H. Zhang, J. Tang, Z. Wang, X. Li, Biochar prepared from co-pyrolysis of municipal sewage sludge and tea waste for the adsorption of methylene blue from aqueous solutions: kinetics, isotherm, thermodynamic and mechanism, J. Mol. Liq., 220 (2016) 432–441.

[17] R.M. Novais, J. Carvalheiras, D.M. Tobaldi, M.P. Seabra, R.C. Pullar, J.A. Labrincha, Synthesis of porous biomass fly ash-based geopolymer spheres for efficient removal of methylene blue from wastewaters, J. Cleaner Prod., 207 (2019) 350–362.

[18] G. García-Rosales, A. Colín-Cruz, Biosorption of lead by maize (*Zea mays*) stalk sponge, J. Environ. Manage., 91 (2010) 2079–2086.

[19] D. Krishna Veni, P. Kannan, T.N. Jebakumar Immanuel Edison, A. Senthilkumar, Biochar from green waste for phosphate removal with subsequent disposal, Waste Manage., 68 (2017) 752–759.

[20] L.I. Li, Y.-c. Lu, Y. Liu, H.-w. Sun, Z.-y. Liang, Adsorption mechanisms of cadmium (II) on biochars derived from corn straw, J. Agro-Environ. Sci., 31 (2012) 2277–2283.

[21] Y.-Y. Wang, Y.-X. Liu, H.-H. Lu, R.-Q. Yang, S.-M. Yang, Competitive adsorption of Pb(II), Cu(II), and Zn(II) ions onto hydroxyapatite-biochar nanocomposite in aqueous solutions, J. Solid State Chem., 261 (2018) 53–61.

[22] F. Jing, S.P. Sohi, Y. Liu, J. Chen, Insight into mechanism of aged biochar for adsorption of PAEs: reciprocal effects of ageing and coexisting Cd^{2+}, Environ. Pollut., 242 (2018) 1098–1107.

[23] B. Hayati, A. Maleki, F. Najafi, H. Daraei, F. Gharibi, G. McKay, Super high removal capacities of heavy metals (Pb^{2+} and Cu^{2+}) using CNT dendrimer, J. Hazard. Mater., 336 (2017) 146–157.

[24] Y. Zhu, J. Hu, J. Wang, Competitive adsorption of Pb(II), Cu(II) and Zn(II) onto xanthate-modified magnetic chitosan, J. Hazard. Mater., 221–222 (2012) 155–161.

[25] P.N. Diagboya, B.I. Olu-Owolabi, K.O. Adebowale, Effects of time, soil organic matter, and iron oxides on the relative retention and redistribution of lead, cadmium, and copper on soils, Environ. Sci. Pollut. Res. Int., 22 (2015) 10331–10339.

[26] M.A. Hossain, H.H. Ngo, W.S. Guo, L.D. Nghiem, F.I. Hai, S. Vigneswaran, T.V. Nguyen, Competitive adsorption of metals on cabbage waste from multi-metal solutions, Bioresour. Technol., 160 (2014) 79–88.

[27] H.J. Hong, B.G. Kim, J. Ryu, I.S. Park, K.S. Chung, S.M. Lee, J.B. Lee, H.S. Jeong, H. Kim, T. Ryu, Preparation of highly stable zeolite-alginate foam composite for strontium(^{90}Sr) removal from seawater and evaluation of Sr adsorption performance, J. Environ. Manage., 205 (2018) 192–200.

[28] X. He, T. Zhang, H. Ren, G. Li, L. Ding, L. Pawlowski, Phosphorus recovery from biogas slurry by ultrasound/H_2O_2 digestion coupled with HFO/biochar adsorption process, Waste Manage., 60 (2017) 219–229.

[29] C. Nguyen, D.D. Do, The Dubinin–Radushkevich equation and the underlying microscopic adsorption description, Carbon, 39 (2001) 1327–1336.

[30] H. Liu, C. Wang, J. Liu, B. Wang, H. Sun, Competitive adsorption of Cd(II), Zn(II) and Ni(II) from their binary and ternary acidic systems using tourmaline, J. Environ. Manage., 128 (2013) 727–734.

[31] R. Ahmad, S. Haseeb, Adsorption of Pb(II) on *Mentha piperita* carbon (MTC) in single and quaternary systems, Arabian J. Chem., 10 (2017) S412–S421.

[32] H. Du, W. Chen, P. Cai, X. Rong, X. Feng, Q. Huang, Competitive adsorption of Pb and Cd on bacteria-montmorillonite composite, Environ. Pollut., 218 (2016) 168–175.

[33] C. Fan, K. Li, J. Li, D. Ying, Y. Wang, J. Jia, Comparative and competitive adsorption of Pb(II) and Cu(II) using tetraethylenepentamine modified chitosan/$CoFe_2O_4$ particles, J. Hazard. Mater., 326 (2017) 211–220.

[34] J.-H. Park, Y.S. Ok, S.-H. Kim, J.-S. Cho, J.-S. Heo, R.D. Delaune, D.-C. Seo, Competitive adsorption of heavy metals onto sesame straw biochar in aqueous solutions, Chemosphere, 142 (2016) 77–83.

[35] M. Fan, S. Tong, Importance and contribution of activated carbon mesopore to the adsorption of Pb(II) and Cd(II) from aqueous solution, Funct. Mater., 49 (2018) 2093–2102.

[36] L. de Pablo, M.L. Chávez, M. Abatal, Adsorption of heavy metals in acid to alkaline environments by montmorillonite and Ca-montmorillonite, Chem. Eng. J., 171 (2011) 1276–1286.

[37] E.R. Nightingale Jr., Phenomenological theory of ion solvation. Effective radii of hydrated ions, J. Phys. Chem., 136 (1967) 566–567.

[38] C. Ding, W. Cheng, X. Wang, Z.-Y. Wu, Y. Sun, C. Chen, X. Wang, S.-H. Yu, Competitive sorption of Pb(II), Cu(II) and Ni(II) on carbonaceous nanofibers: a spectroscopic and modeling approach, J. Hazard. Mater., 313 (2016) 253–261.

[39] C. Mahamadi, T. Nharingo, Competitive adsorption of Pb^{2+}, Cd^{2+} and Zn^{2+} ions onto *Eichhornia crassipes* in binary and ternary systems, Bioresour. Technol., 101 (2010) 859–864.

[40] S. Chen, Q. Yue, B. Gao, Q. Li, X. Xu, K. Fu, Adsorption of hexavalent chromium from aqueous solution by modified corn stalk: a fixed-bed column study, Bioresour. Technol., 113 (2012) 114–120.

[41] V. Vinodhini, N. Das, Packed bed column studies on Cr (VI) removal from tannery wastewater by neem sawdust, Desalination, 264 (2010) 9–14.

[42] S.K. Maji, A. Pal, T. Pal, A. Adak, Modeling and fixed bed column adsorption of As(III) on laterite soil, Sep. Purif. Technol., 56 (2007) 284–290.

[43] Y. Dong, H. Lin, Competitive adsorption of Pb(II) and Zn(II) from aqueous solution by modified beer lees in a fixed bed column, Process Saf. Environ. Prot., 111 (2017) 263–269.

[44] L. Sheng, Y. Zhang, F. Tang, S. Liu, Mesoporous/microporous silica materials: preparation from natural sands and highly efficient fixed-bed adsorption of methylene blue in wastewater, Microporous Mesoporous Mater., 257 (2018) 9–18.